学位論文

High glucose induces platelet derived growth factor-C via carbohydrate response element binding protein in glomerular mesangial cells

（ 高グルコースは腎メサンギウム細胞においてグルコース応答性転写因子 ChREBP を介して血小板由来成長因子 PDGF-C の発現を誘導する ）

旭川医科大学大学院医学系研究科博士課程医学専攻

橘内 博哉

（ 牧野 雄一、坂上 英充、 水元 克俊、 柳町 剛司、
Kuralay Atageldiyeva、竹田 安孝、 藤田 征弘、
安孫子 亜津子、 滝山 由美、 羽田 勝計 ）

High glucose induces platelet derived growth factor-C via carbohydrate response element binding protein in glomerular mesangial cells

Hiroya Kitsunai, Yuichi Makino, Hidemitsu Sakagami, Katsutoshi Mizumoto, Tsuyoshi Yanagimachi, Kuralay Atageldiyeva, Yasutaka Takeda, Yukihiro Fujita, Atsuko Abiko, Yumi Takiyama, and Masakazu Haneda

Abstract

Persistent high concentration of glucose causes cellular stress and tissue damage including microvascular complications in diabetes via derangement of gene expressions. We previously reported that high glucose activates hypoxia-inducible factor-1α and downstream gene expression in mesangial cells, leading to an extracellular matrix expansion in diabetic glomeruli. A glucose responsive transcription factor carbohydrate response element binding protein (ChREBP) is a key mediator for such perturbation of gene regulation by high glucose. To provide more insight into glucose-mediated gene regulation in mesangial cells, we performed chromatin immunoprecipitation with anti-ChREBP antibodies followed by DNA microarray analysis (ChIP-chip) and identified platelet derived growth factor C (PDGF-C) as a novel target gene of ChREBP in mesangial cells. In the streptozotocin-induced diabetic mouse model, glomerular mesangial cells had a significant increase in PDGF-C expression along the disease course of diabetes. In cultured mesangial cells, high glucose enhanced expression of PDGF-C and knock-down of ChREBP abrogated such induction response. Upregulated PDGF-C encouraged mesangial cells to produce type IV collagen and type VI collagen possibly via an autocrine mechanism and reduction of cellular PDGF-C compromised induction of those fibrotic extracellular matrixes by high glucose. Interestingly, urinary PDGF-C level in diabetic model mice was significantly elevated in a similar fashion to urinary albumin. Taken together, we hypothesis that high glucose-mediated induction of PDGF-C via ChREBP in mesangial cells contributes to the development of the glomerular mesangial expansion in diabetes, which may provide a platform for novel predictive and therapeutic strategies for diabetic nephropathy.

Introduction

Diabetic nephropathy (DN) is a major chronic microvascular complication of diabetes mellitus (DM) and is an important cause of increased morbidity and mortality in patients with DM. Previous studies including Diabetes Control and Complications Trial in patients with type 1 diabetes [1] and UK Prospective Diabetes Study in patients with type 2 diabetes [2] indicate a causal link between the degree of glycemic control in patients with diabetes and the development and progression of DN. In addition, Action to Control Cardiovascular Risk in Diabetes (ACCORD) trial, recent large intervention trial aiming at tight glycemic control, demonstrated a reduction in the risk of new-onset of albuminuria, surrogate outcomes of DN, by a strict glycemic control [3]. Similarly, a post-hoc analysis of the Action in Diabetes and Vascular Disease (ADVANCE) study revealed intensive glucose control reduced the risk of end stage renal disease and new onset of albuminuria [4]. Obviously, a remedy of hyperglycemia could prevent the initiation and development of DN thus elucidation of the hyperglycemia-related molecular pathogenesis of organ damage would provide further insight into therapeutic strategies for DN.

The histopathological hallmarks of DN are increased thickness of the glomerular basement membrane and an excessive accumulation of extracellular matrix proteins in the glomeruli [5]. Multiple mechanisms including hyperglycemia-induced metabolic and hemodynamic changes [6] and genetic predisposition [7] have been shown to induce functional changes in glomerular mesangial cells. High glucose is a primary initiating factor of hyper-activation of metabolic pathways for polyols [8] and hexosamines [9], non-enzymatic glycation that generates advanced glycation end products [10] and reactive oxygen species (ROS) [11], activation of protein kinase C (PKC) [12], and production of cytokines such as transforming growth factor-β1 (TGF-β1) and connective tissue growth factor (CTGF) [13], all of which cause overproduction of matrix proteins by mesangial cells

[14]. High glucose also induces inhibitors of matrix-degrading enzymes including plasminogen activator inhibitor-1 (PAI-1), which as well lead to an accumulation of extracellular matrix proteins [15].

Recently, several factors including SMAD1, SMAD3, STAT1, STAT3, Nrf2, and NFκB are shown to participate in gene regulation in kidney of diabetic patient or diabetic animal models [16-20]. Such transcriptional regulators possibly downstream of hyperglycemia thus may emerge as attractive targets in therapeutic attempts. In this line, we previously demonstrated an activation of the hypoxia-inducible transcription factor-1α (HIF-1α) by high glucose without an aid of hypoxia in glomerular mesangial cells [21]. In the streptozotocin (STZ) -induced and genetic db/db diabetic mice models, glomerular mesangial cells had a significant increase in HIF-1α expression in the nucleus. In cultured mesangial cells, high glucose enhanced the expression of HIF-1α and genes such as CTGF and PAI-1 which are known to be involved in extracellular matrix accumulation in diabetic glomeruli. Knock down of HIF-1α in mesangial cells abrogated high glucose-induced increase in those genes expression, indicating a previously unknown role of HIF-1α in development of glomerulopathy in response to high glucose. Of note, a glucose-responsive carbohydrate response element binding protein (ChREBP) was found to upregulate HIF-1α mRNA expression via direct binding to promoter of HIF-1α gene, providing a mechanism for diverse output of glucose signaling and a novel link between high glucose and diabetic kidney injury.

ChREBP is a basic helix-loop-helix/leucine zipper transcription factor of approximately 100 kDa, also termed MondoB or Williams - Beuren syndrome critical region gene 14 (WBSCR14). Originally cloned from liver tissue, ChREBP up-regulates genes involved in glycolysis and fatty acid synthesis in a glucose-dependent manner [22]. ChREBP also is expressed in several metabolically relevant tissues, including adipocytes, pancreatic

β-cells, and certain cancer cells, indicating a wide variety role and physiological importance of ChREBP [23-25]. Upon activation by glucose ChREBP translocates from the cytosol into the nucleus [26]. In the nucleus, ChREBP forms a heterodimer with Max-like protein X (Mlx) to bind to the carbohydrate response element (ChRE) for transcriptional regulation of its target genes [27-29]. Jeong et al. demonstrated ChRE motif search and identified 1153 ChREBP binding sites and 783 target genes using the chromatin from HepG2, a human hepatocellular carcinoma cell line. Gene ontology analysis showed that ChREBP target genes in hepatocyte are particularly associated with lipid, fatty acid and steroid metabolism [30]. Genes regulated in mesangial cells via ChREBP, however, have not been documented.

To provide more insight into glucose-responsive gene regulation in mesangial cells, we in the present study performed genome-wide search for ChREBP binding site employing the chromatin from human mesangial cells exposed to high glucose and demonstrated possible role of ChREBP in profibrotic response of mesangial cells to high glucose ambience.

Materials and Methods

Reagents and cells

Human mesangial cells were obtained from Lonza (Basel, Switzerland). The immortalized mouse mesangial cells, SV40 MES 13, were from American Type Culture Collection (Manassas, VA). Recombinant human PDGF-C was obtained from PeproTech (Rocky Hill, NJ). 6, 7-Dimethyl-2-phenylquinoxaline (AG1295) was purchased from Calbiochem (Darmstadt, Germany).

Cell culture

Before each assay, the cells were serum starved for 12 h in the media containing 0.2% bovine serum albumin. Cellular responses to different glucose concentrations were determined in the serum-free culture media.

Chromatin immunoprecipitation and microarray

Human mesangial cells cultured in 5.6 mM or 25 mM glucose were cross-linked with formaldehyde. Cross-linking was stopped by the addition of glycine. Nuclei were collected and resuspended in sonication buffer and sonicated using Bioruptor UCD-250 (COSMO BIO, Tokyo, Japan). After sonication, the chromatin solution was incubated with Dynabeads protein G and rabbit anti-ChREBP (NB400-135, Novus biologicals, Littleton, CO) or rabbit normal IgG at 4℃ overnight. Antibody-bound complexes were obtained and DNA fragments extricated from these complexes were purified using the ChIP-IT Express Kit (Active Motif, Carlsbad, CA). The purified immunoprecipitated DNA samples were analyzed by microarray hybridization (ChIP-chip) assays using Affymetrix GeneChip Human 2.0R Array Set (Santa Clara, CA). PCR analysis was performed using primers flanking the ChRE within the PDGF-C gene promoter: human, 5’-TAGTCTGAAATGAAACACACA-3’ (forward) and

5’-ACTTTTCTGACTCTCTGCTTG-3’ (reverse), mouse,

5’-CCAACTACAAGATGCACACA-3’ (forward) and,

5’-CAATAGTGAGATCGAGACTG-3’ (reverse).

Quantitative PCR analyses

Total RNA was reverse-transcribed into cDNA with oligo dT primers using Superscript II reverse transcriptase (Invitrogen, Carlsbad, CA). Quantitative PCR was performed using β-actin as internal standard on the basis of TaqMan Gene Expression Assays (Applied Biosystems, Foster City, CA).

Immunobloting

The proteins extracted from whole-cell were separated on sodium dodecyl sulfate-polyacrylamide gel electrophoresis and transferred to PVDF membrane. For western blots the following primary antibodies were used; anti-PDGF-C (ab93899, Abcam, Cambridge, U.K.), anti-Collagen IV (ab6586, Abcam), anti-Collagen VI (ab6588, Abcam) and anti-β-actin (sc-47778, Santa Cruz, Dallas, Texas) diluted 1:1000. Primary antibodies were incubated in Tris-buffered saline with 1% milk. Secondary antibodies conjugated with horseradish peroxidase (GE Healthcare, Buckinghamshire, UK) diluted 1:20000 and the electrochemiluminescent detection system (GE Healthcare) was used for visualization. For the semi-quantitative analyses, the band densities were measured using Multigauge ver. 2.2 (Fujifilm, Tokyo, Japan).

Gene knockdown by shRNA

To knockdown ChREBP or PDGF-C, mouse mesangial cells were transfected with the small hairpin RNA (shRNA) specifically targeting ChREBP or PDGF-C. The sequences of

the RNA are as follows: ChREBP sense, 5’-GGCCUCAAGUUGCUAUGCCTT-3’ and antisense, 5’-GGCAUAGCAACUUGAGGCCTT-3’; PDGF-C sense, 5’-GAAATATGGTGCTGGTGTG-3’ and antisense, 5’-CACACCAGCACCATATTTCTT-3’. shRNA with a non-targeting scrambled sequence was used as a control.

Animals

Male C57BL/6 mice, 6 weeks old, weighing 20-22 g were rendered diabetic by the intraperitoneal injection of 50mg per kg body weight streptozotocin (STZ) in citrate buffer, pH 4.5, for 5 consecutive days. The diabetic state was confirmed 2 weeks after final injection by measurement of blood glucose level. All mice that were given STZ had a blood glucose concentration exceeding 300mg/dl and were considered diabetic. Genetically diabetic male BKS.Cg-+Leprdb /+Leprdb/J (db/db) mice and their age-matched heterozygous non-diabetic male littermates BKS.Cg-Dock7m+/+Leprdb/J (db/m) mice were obtained from Charles River Laboratories Japan (Yokohama, Japan). All animal experiments were conducted according to the institutional guidelines for animal care and welfare.

Histological analyses of the kidney

The kidneys of the mice were fixed in 4% paraformaldehyde, dehydrated and embedded in paraffin. Then, 4 μm sections were used for immunohistochemical analysis. Immunohistochemical analyses with polyclonal anti-PDGF-C antibody (AF1447, R & D systems, Minneapolis, MN) were carried out as described [31]. For semiquantitative analyses, 30 glomeruli were subjected to counting of PDGF-C-positive cells to determine the number of positive cells per glomerulus and the ratio of positive cells to the total number of the counted cells. Immunofluorescent analyses were performed by incubation with polyclonal anti-PDGF-C antibody (sc-33190, Santa Cruz), anti-α-smooth muscle actinin antibody

(ab7817, Abcam), monoclonal anti-CD34 antibody (ab8158, Abcam), or polyclonal anti-Nephrin antibody (GP-N2, PROGEN Biotechnik GmbH, Heidelberg, Germany) followed by fluorescence-conjugated secondary antibodies. Staining with 4, 6-diamidino-2-phenylindole (DAPI) was performed to identify the nucleus.

Enzyme-Linked Immunosorbent Assay

The spot urine samples and random serum samples were obtained from the mice. Urinary PDGF-C level and plasma PDGF-C level were measured using ELISA Kit for Platelet Derived Growth Factor C (PDGFC) (SEC920Mu, Uscn Life Science, Wuhan, China). Urinary albumin level was measured using Albumin, Mouse Urine, ELISA Kit, Albuwell M (1011, Exocell, Philadelphia, PA). The values of their urinary PDGF-C levels and albumin levels were expressed as values corrected by the urinary creatinine concentration measured by Creatinine Companion Kit (1012, Exocell).

Statistical analysis

All data are presented as means ± SD from the experiments with repetitions as indicated. Comparisons between two groups were analyzed using t-test. One-factor analysis of variance and two-factor factorial analysis of variance followed by the Bonferroni/Dunn test were carried out to determine significant differences in multiple comparisons. The P-values of <0.05 were considered to be significant.

Results

Genome-wide chromatin immunoprecipitation analysis identified platelet derived growth factor-C (PDGF-C) as a target gene of ChREBP in glomerular mesangial cells in high glucose ambience

To explore the role of ChREBP in transcriptional regulation in glomerular mesangial cells in diabetic circumstances, we performed a genome location and expression profiling analyses to identify genes directly regulated by ChREBP. To this end, we treated primary human mesangial cells with high level of glucose (25 mM) for 48h then performed chromatin immunoprecipitation (ChIP) with anti-ChREBP antibodies followed by microarray hybridization (ChIP-chip) assays to assess the extent of promoter occupancy by ChREBP at a genome-wide level. As a control, we carried out parallel ChIP-chip experiments employing mesangial cells treated with a media containing normal level of glucose (5.6 mM). Among a total of 139 genes selectively enriched with anti-ChREBP antibodies in mesangial cells cultured under high glucose conditions (Table 1), platelet derived growth factor-C (PDGF-C) gene was found to harbor ChREBP-binding site within 5 kbp of 5'-flanking region. Accordingly, sequence analysis of human *PDGF-C* gene revealed the presence of carbohydrate response element (ChRE)-like sequence at approximately 1.5 kbp upstream of transcriptional start site (Fig. 1A). Given these facts, we performed conventional ChIP analysis and demonstrated ChREBP binding to this sequence in human mesangial cells cultured in high glucose media (Fig. 1B). To validate the results of ChIP-chip assay, we determined PDGF-C expression in human mesangial cells in response to high glucose stimulation. Quantitative PCR demonstrated 1.3-fold induction of *PDGF-C* mRNA in human measangial cells cultured in high glucose-media compared to the cells in normal glucose-media (Fig. 1C). Similarly, immunoblot analyses showed about 1.9-fold increase in PDGF-C protein level in response to high glucose media compared to normal glucose (Fig.

1D). Analogy to human cells, mouse mesangial cells showed induction response of *Pdgf-c* mRNA upon stimulation with glucose in a concentration-dependent manner (Fig. 1E). Consistently, protein levels of PDGF-C were dose-dependently upregulated by glucose; 11.2 mM and higher concentrations of glucose gradually induced significant increase of PDGF-C expression (Fig. 1F). In support of these observations, sequence analyses found the ChRE-like sequence in the first intron of mouse *Pdgf-c* gene (Fig. 1G) and ChIP assays adopting mouse mesangial cells demonstrated high glucose-dependent binding of ChREBP to the site (Fig. 1H). Moreover, the shRNA-mediated reduction of cellular ChREBP level in mouse mesangial cells resulted in an impairment of basal and high glucose-induced *Pdgf-c* mRNA expression (Fig. 1I). These results indicate that high glucose upregulates PDGF-C expression in glomerular mesangial cells via direct regulation by ChREBP.

PDGF-C expression is elevated in glomerular mesangial cells of diabetic model mice

We next examined the expression of PDGF-C in the glomeruli of diabetic model mice by immunohistochemical methods. Kidneys from the diabetic or non-diabetic mice after streptozotocin (STZ) or vehicle injection were tested for PDGF-C staining. At 4 wk after treatment, a modest staining of PDGF-C was observed in glomeruli of both STZ- and vehicle-treated mice (Fig. 2A). In the glomeruli of mice at 8, 12 and 16 wk after STZ introduction PDGF-C signals were higher than that in the glomeruli of the control mice (Fig. 2A). At 20 wk after STZ injection, PDGF-C staining was scarcely detectable as well as control mice at the same time point (Fig. 2A). In a series of semi-quantitative analyses, PDGF-C positive cells were found with significantly higher incidence in diabetic kidney compared to the control mice between 8 and 16 wk after STZ injections. The number of PDGF-C positive cells was highest at 12 wk after introduction of STZ (Fig. 2B). The ratio of the numbers of PDGF-C-positive cells to that of total glomerular cells was significantly

increased in the same time course in diabetic mice (Fig. 2C), therefore cellular hyperplasia does not explain the increase in the number of PDGF-C positive cells. To characterize the cells expressing PDGF-C in the glomeruli, we performed co-immunofluorescent staining. The cells with positive staining for PDGF-C or α-smooth muscle actinin (α-SMA), which is often induced in mesangial cells in injured glomeruli, were increased in STZ-induced diabetic mice (Fig. 3A). When the fluoro-microscopic photographs were merged, a certain fraction of PDGF-C staining co-localized with α-SMA staining, indicating an increase of PDGF-C in the mesangial cells in diabetic kidneys. Co-staining of PDGF-C and nephrin, a marker of podocytes, depicted only a few overlaps of PDGF-C and nephrin signals (Fig. 3B). The costaining with CD34, a marker of vascular endothelial cells, show a seldom presence of induced PDGF-C in endothelial cells in the glomeruli (Fig. 3C). Semiquantitative summary of these co-immunofluorescent studies revealed that PDGF-C is most abundantly expressed in the mesangial cells in the diabetic glomeruli (Fig. 3D). These results suggest that PDGF-C may participate in pathology of glomerular mesangial cells in diabetic kidney. On the other hand, in the tubulointerstitial area, PDGF-C expression was observed only in distal tubules. The extent of PDGF-C staining was the same in diabetic and non-diabetic mice through the time course after animal model induction (Fig. 4), indicating that PDGF-C is constitutively expressed in the distal tubules.

High glucose-induced PDGF-C upregulates genes encoding Collagen IV and Collagen VI in mesangial cells

Recent studies have shown that PDGF-C has critical roles in mitogenic and fibrogenic changes in various disease conditions including lung fibrosis or liver cirrhosis. In such context, PDGF-C is known to participate in regulation of genes encoding type IV or type VI collagens. Therefore, we investigated the role of high glucose-induced PDGF-C in

mesangial cells with respect to an accumulation of extracellular matrix or fibrotic components. For this purpose, we generated mouse mesangial cells in which PDGF-C expression is compromised by stable integration of PDGF-C shRNA expression vector. Culture of mouse mesangial cells with a medium containing high concentration (25 mM) of glucose induces higher expression of mouse *Col4a1* mRNA or *Col6a1* mRNA compared to the cells in a medium with normal concentration (5.6 mM) of glucose (Fig. 5A; lane 3 compared to lane 1, Fig. 5B; lane 3 compared to lane 1, respectively). Knockdown of PDGF-C abrogated both basal and high glucose-induced expression of mouse *Col4a1* mRNA and *Col6a1* mRNA (Fig. 5A; lanes 4 and 2 compared to lanes 3 and 1, Fig. 5B; lanes 4 and 2 compared to lanes 3 and 1, respectively). Similarly, mouse type IV collagen (mCol IV) and type VI collagen (mCol VI) proteins were upregulated in mesangial cells exposed to high glucose (Fig. 5C; lane 3 compared to lane 1, Fig. 5D; lane 3 compared to lane 1, respectively) and reduction of cellular PDGF-C impaired such cellular induction response to high glucose (Fig. 5C; lane 4 compared to lane 3, Fig. 5D; lane 4 compared to lane 3, respectively). These results indicate the critical role of PDGF-C in high glucose-mediated induction of type IV collagen and type VI collagen in glomerular mesangial cells. In an agreement with this hypothesis, addition of AG1295, an inhibitor of PDGF-α and -β receptors to culture medium abolished high glucose-induced upregulation of *COL4A1* and *COL6A1* mRNA expression in human mesangial cells (Fig. 6A and B, compared lane 3 to lane 2). Moreover, stimulation of human mesangial cells with PDGF-C caused an induction of *COL4A1* and *COL6A1* mRNA (Fig. 7 A and B). Taken together, PDGF-C and the cognate receptor-mediated signals are crucially involved in an augmentation of extracellular matrix protein production by mesangial cells in high glucose ambience.

Urinary PDGF-C level is increased in diabetic model mice

Finally, we determined levels of urinary PDGF-C in diabetic model mice. In a type-1 diabetes model mice induced by STZ treatment, urinary albumin excretion was detectable at 8 wk after treatment then significantly increased compared to control group at 12 wk or later, indicating a presence of possible kidney damage in the model mice (Fig. 8A). Urinary PDGF-C level was significantly elevated at 8 wk and reached a peak at 12 wk after induction (Fig. 8B), showing similar or earlier profile of urinary appearance to that of albumin. In contrast, plasma PDGF-C level was not elevated even at 12 wk after STZ-treatment (Fig. 8E), indicating that the increase in urinary PDGF-C may reflect local events in diabetic kidney. A genetic model mice resembling type-2 diabetes, db/db mice, demonstrated a significant albuminuria at 14 wk after birth compared to the control db/m mice and maximal level of albuminuria at 18 wk (Fig. 8C). An increment of urinary PDGF-C level was significant in diabetic db/db mice compared to the control mice at 10 wk after birth. Urinary PDGF-C levels peaked at 14 wk and were significantly higher afterward than control mice (Fig. 8D). Similarly to the case of STZ-induced diabetic mice, plasma PDGF-C level in db/db mice was comparable to the control mice at 14 wk (Fig. 8F). In conclusion, urinary PDGF-C level was elevated in diabetic mice in a similar fashion to that of albumin, an established early marker of diabetic kidney damage, indicating a possible adoption of urinary PDGF-C in a prediction of kidney injury in diabetes.

Discussion

Gene regulation by high glucose is an important issue in molecular patho-physiology of metabolic diseases including diabetes mellitus and its complications. High glucose and its metabolites have been shown to operate in direct activation of a fraction of transcription factors such includes ChREBP [32, 33]. In the present study, we aimed to identify ChREBP target genes in mesangial cells and their roles on genome-wide scale by means of ChIP-chip analyses for further understanding of the mechanism underlying diabetic glomerulopathy. Subtraction of ChREBP binding sites in mesangial cells cultured in the medium with normal glucose concentration from that in high glucose culture revealed high glucose-dependent binding of ChREBP to 139 sites across the genome, 15% of which are located in potential gene regulatory regions of 5kb spanning 5'- or 3'-UTR. Among them, *PDGF-C* gene was found to carry cis-aligned ChREBP-binding site at approximately 1.5 kbp upstream of transcriptional start site. Similarly, there was a ChREBP-binding sequence in the first intron of mouse *Pdgf-c* gene as well. Quantitative PCR and immunoblot analyses revealed high glucose-dependent upregulation of PDGF-C expression in either human or mouse mesangial cells. ChIP analyses reproduced a direct binding of ChREBP to both human and mouse PDGF-C gene in the presence of stimulation with high glucose, indicating an involvement of ChREBP in glucose-mediated induction of PDGF-C in mesangial cells over the species.

The PDGF system, comprising four isoforms (PDGF-A, -B, -C, and -D) and two receptor chains (PDGFR-α and -β), has been shown to play pivotal roles in wound healing, atherosclerosis, organ fibrosis, and cancers. Particularly, PDGF-C is a potent mitogen for fibroblasts in vitro. Recent studies have shown that PDGF-C has critical roles in mitogenic and fibrogenic changes in various disease conditions. A mouse model in which transgenic overexpression of PDGF-C in the heart demonstrated fibroblast proliferation, cardiac fibrosis, hypertrophy, and cardiomyopathy [34, 35]. Liver-specific PDGF-C overexpression by the

transgene caused liver fibrosis and hepatocellular carcinoma [36]. A local PDGF-C overexpression in the lung developed massive mesenchymal cell hyperplasia and died from respiratory insufficiency immediately after birth [37].

Despite little is known about the functional role of PDGF-C within the kidney, expression of PDGF-C in the normal kidney is observed at arterial smooth muscle cells and collecting-duct epithelial cells in the rat [38], and parietal epithelial cells in the glomerulus, distal tubular epithelial cells, arterial epithelial cells in human kidneys [39]. In the renal disease models, upregulation of PDGF-C was identified within the mesangium in rat experimental mesangioproliferative glomerulonephritis [38], and in podocytes at sites of focal glomerular injury in a rat model of spontaneous glomerulosclerosis [38]. In human disease conditions, a marked upregulation of glomerular PDGF-C protein was seen in membranous nephropathy and transplant glomerulopathy with a prominent positivity of podocytes and additional expression in individual mesangial cells [39]. In membranous nephropathy, increased glomerular PDGF-C protein expression was due to increased mRNA synthesis compared to normal kidney. PDGF-C was also detected in fibrosing tubulointerstitial lesions in variety of human kidney diseases [39]. Accumulated PDGF-C in the kidney under disease conditions is potentially pathogenic since administration of a specific neutralizing anti-PDGF-C antiserum or disruption of PDGF-C gene in mice unilateral ureteral obstruction model exhibited a striking reduction of tubulointerstitial fibrotic lesions, a remarkable reduction of interstitial myofibroblast accumulation, and a decrease in leukocyte infiltration [40]. However, PDGF-C expression in diabetic kidney disease has not been well documented. We in the present study found an increase in PDGF-C expression in the glomerulus of the STZ-induced diabetic model mice by immunohistochemical methods. In the tubulointersitial area, we only detected basal expression of PDGF-C in distal tubular epithelial cells, possibly as a constitutive expression in the normal kidney. The increment of PDGF-C expression in the

diabetic glomeruli was peaked at 12 wk after induction of diabetes and recovered to the basal level at 20 wk. Although the pathological relevance of this time-course is not clear at this moment, transient induction of mRNAs for CTGF, TGF-β, and fibronectin was observed in the glomeruli from STZ-induced rat diabetic model as well [41]. Our co-immunofluorescent analyses indicated that mesangial cell is a major site of PDGF-C expression in the glomeruli in diabetes. Consistently, in cultured mesangial cells PDGF-C was induced by high glucose at mRNA levels. Knock-down of PDGF-C gene in the mesangial cells abolished high glucose-induced accumulation of type IV collagen and type VI collagen, suggesting an involvement of PDGF-C in such fibrotic extracellular matrix production by the mesangial cells. In addition, stimulation of the mesangial cells with recombinant PDGF-C promoted *COL4A1* and *COL6A1* mRNA expression within the cells. Moreover, mesangial cells express the cognate receptor PDGFR-α (data not shown) and specific inhibition of PDGF receptor by AG1295 diminished high glucose-mediated induction of *COL4A1* and *COL6A1* mRNA, indicating a possible autocrine regulation of pathologic extracellular matrix expansion via PDGF-C by mesangial cells under diabetic circumstances. Interestingly, previous studies reported elevated expression of PDGF-B and its main receptor PDGFR-β in the glomerular cells including mesangial cells of diabetic patient [42] and of STZ-induced diabetic rat [43] with limited information concerning the function of those elevated molecules. It has been known that activated PDGFR-α (main receptor for PDGF-C) and PDGFR-β induce overlapping and different effects on target cells, therefore, redundant or distinct roles of PDGF-C and PDGF-B and their receptors in diabetic glomeruli would be an interesting matter of debate.

On the other hand, PDGF-C produced by glomerular mesangial cells may exert its roles via a paracrine mechanism. Indeed, analyses of various human kidney tubulointerstitial diseases revealed typically a finely granular immunohistochemical signal of PDGF-C in

fibrosing area and the absence of intracellular localization of PDGF-C in interstitial cells [39], indicating a delivery of PDGF-C from somewhere else. In this aspect, not only tissue interstitial fluid but also the glomerular filtrate might be such candidates of the transit route for PDGF-C, as we demonstrated elevation of urinary PDGF-C in diabetic model mice. Interestingly, infusion of PDGF-C accelerated glomerular capillary repair via at least direct effect on the glomerular endothelium expressing PDGFR-α in the early mesangiolytic phase of mesangioproliferative glomerulonephritis in rats [44]. Therefore, such paracrine (or endocrine) mode of PDGF-C action may constitute a diverse e.g., pathological or beneficial roles in kidney disease.

We also demonstrated that urinary PDGF-C level is upregulated in the disease course of both type 1 and type 2 diabetic animal models. The elevation of PDGF-C in the urine seemed more or less earlier than the significant urinary excretion of albumin. Even though plasma PDGF-C level in diabetic animal was comparable to that in control mice, the origin of the elevated PDGF-C in the urine is still elusive. Information on the behavior of PDGF-C after production by mesangial cells e.g. excretion and absorption at the tubules or on the interfering substances in the urine or plasma for enzyme-linked immunosorbent assays are obviously required to consider if urinary PDGF-C is originated from kidneys. Nevertheless detection of albuminuria currently crucially contributes to the diagnosis of diabetic nephropathy, the prediction of a decrease in GFR and the incidence of cardiovascular diseases, albuminuria is not a perfect biomarker [45]. For examples, some diabetic patients develop biopsy-proven diabetic nephropathy in the absence of albuminuria [46]. Thus, there has been a recent effort to identify new biomarkers, favorably by non-invasive methods, which reflect kidney function, early injury, and/or repair that ultimately can relate to progression or regression of damage. The emerging candidates of biomarker for diabetic nephropathy include liver-type fatty acid-binding protein [47], retinal venular caliber [48], and urinary

exosomal microRNAs [49]. In this aspect, measurement of urinary PDGF-C in diabetic patient is of a great interest and now under preparations.

In conclusion, we propose a novel axis of ChREBP and PDGF-C in extracellular matrix deposition, which might contribute to the development of glomerulopathy in diabetic conditions. Pharmacological inhibition or gene silencing in this axis seemed to ameliorate concomitant fibrotic gene regulation. To elucidate a value of targeting this cascade in therapeutic and diagnostic purpose, further analyses with clinical specimens are clearly needed.

Reference

1. Shamoon H, Duffy H, Fleischer N, et al. The effect of intensive treatment of diabetes on the development and progression of long-term complications in insulin-dependent diabetes mellitus. New England Journal of Medicine, 1993; 329 (14): 977-86.

2. Turner R. Intensive blood-glucose control with sulphonylureas or insulin compared with conventional treatment and risk of complications in patients with type 2 diabetes (UKPDS 33). The Lancet, 1998; 352 (9131): 837-53.

3. Ismail-Beigi F, Craven T, Banerji MA, et al. Effect of intensive treatment of hyperglycaemia on microvascular outcomes in type 2 diabetes: an analysis of the ACCORD randomised trial. Lancet, 2010; 376: 419-30.

4. Perkovic V, Heerspink HL, Chalmers J, et al. Intensive glucose control improves kidney outcomes in patients with type 2 diabetes. Kidney Int, 2013; 83: 517-23.

5. Mason RM, Wahab NA. Extracellular matrix metabolism in diabetic nephropathy. J. Am. Soc. Nephrol, 2003; 14: 1358-73.

6. Gnudi L, Viberti G, Raij L, et al. GLUT-1 overexpression: Link between hemodynamic and metabolic factors in glomerular injury? Hypertension, 2003; 42: 19-24.

7. Mueller PW, Rogus JJ, Cleary PA, et al. Genetics of Kidneys in Diabetes (GoKinD) study: a genetics collection available for identifying genetic susceptibility factors for diabetic nephropathy in type 1 diabetes. J Am Soc Nephrol, 2006; 17: 1782-90.

8. Dunlop M. Aldose reductase and the role of the polyol pathway in diabetic nephropathy. Kidney Int, 2000; 58 (Suppl 77): S3-12.

9. Schleicher ED, Weigert C. Role of the hexosamine biosynthetic pathway in diabetic nephropathy. Kidney Int, 2000; 58 (Suppl 77): S13-8.

10. Forbes JM, Cooper ME, Oldfield MD, et al. Role of advanced glycation end products in diabetic nephropathy. J Am Soc Nephrol, 2003; 14: S254-8.

11. Kiritoshi S, Nishikawa T, Sonoda K, et al. Reactive oxygen species from mitochondria induce cyclooxygenase-2 gene expression in human mesangial cells: potential role in diabetic nephropathy. Diabetes, 2003; 52: 2570-7.

12. Haneda M, Koya D, Kikkawa R. Cellular mechanisms in the development and progression of diabetic nephropathy: activation of the DAG-PKC-ERK pathway. Am J Kidney Dis, 2001; 38 (4 Suppl 1): S178-81.

13. Murphy M, Godson C, Cannon S, et al. Suppression subtractive hybridization identifies high glucose levels as a stimulus for expression of connective tissue growth factor and other genes in human mesangial cells. J Biol Chem, 1999; 274: 5830-4.

14. Haneda M, Koya D, Isono M, et al. Overview of glucose signaling in mesangial cells in diabetic nephropathy. J Am Soc Nephrol, 2003; 14: 1374-82.

15. Lee HB, Ha H. Plasminogen activator inhibitor 1 and diabetic nephropathy. Nephrology, 2005; 10: S11-3.

16. Mima A, Arai H, Matsubara T, et al. Urinary Smad1 is a novel marker to predict later onset of mesangial matrix expansion in diabetic nephropathy. Diabetes, 2008; 57 (6): 1712-22.

17. Hong SW, Isono M, Chen S, et al. Increased glomerular and tubular expression of transforming growth factor-beta1, its type II receptor, and activation of the Smad signaling pathway in the db/db mouse. Am J Pathol, 2001; 158 (5): 1653-63.

18. Berthier CC, Zhang H, Schin M, et al. Enhanced expression of Janus kinase-signal transducer and activator of transcription pathway members in human diabetic nephropathy. Diabetes, 2009; 58 (2): 469-77.

19. Cui W, Bai Y, Miao X, et al. Prevention of diabetic nephropathy by sulforaphane: possible role of Nrf2 upregulation and activation. Oxid Med Cell Longev, 2012; 2012: 821936.

20. Yang B, Hodgkinson A, Oates PJ, et al. High glucose induction of DNA-binding activity of the transcription factor NFkappaB in patients with diabetic nephropathy. Biochim Biophys Acta, 2008; 1782 (5): 295-302.

21. Isoe T, Makino Y, Mizumoto K, et al. High glucose activates HIF-1-mediated signal transduction in glomerular mesangial cells through a carbohydrate response element binding protein. Kidney Int, 2010; 78: 48-59.

22. Uyeda K, Repa JJ. Carbohydrate response element binding protein, ChREBP, a transcription factor coupling hepatic glucose utilization and lipid synthesis. Cell Metab, 2006; 4 (2): 107-10.

23. He Z, Jiang T, Wang Z, et al. Modulation of carbohydrate response element-binding protein gene expression in 3T3-L1 adipocytes and rat adipose tissue. Am J Physiol Endocrinol Metab, 2004; 287 (3): E424-30.

24. Noordeen NA, Khera TK, Sun G, et al. Carbohydrate-responsive element-binding protein (ChREBP) is a negative regulator of ARNT/HIF-1beta gene expression in pancreatic islet beta-cells. Diabetes, 2010; 59 (1): 153-60.

25. Wu L, Chen H, Zhu Y, et al. Flightless I homolog negatively regulates ChREBP activity in cancer cells. Int J Biochem Cell Biol, 2013; 45 (11): 2688-97.

26. Kawaguchi T, Takenoshita M, Kabashima T, Uyeda K. Glucose and cAMP regulate the L-type pyruvate kinase gene by phosphorylation/dephosphorylation of the carbohydrate response element binding protein. Proc Natl Acad Sci USA, 2001; 98: 13710-5.

27. Shih H-M, Liu Z, Towle HC. Two CACGTG motifs with proper spacing dictate the carbohydrate regulation of hepatic gene transcription. J Biol Chem, 1995; 270: 21991-7.

28. Stoeckman AK, Ma L, Towle HC. Mlx is the functional heteromeric partner of the carbohydrate response element-binding protein in glucose regulation of lipogenic enzyme genes. J Biol Chem, 2004; 279: 15662-9.

29. Ma L, Robinson LN, Towle HC. ChREBP*Mlx is the principal mediator of glucose-induced gene expression in the liver. J Biol Chem, 2006; 281: 28721-30.

30. Jeong Y-S, Kim D, Lee YS, et al. Integrated Expression Profiling and Genome-Wide Analysis of ChREBP Targets Reveals the Dual Role for ChREBP in Glucose-Regulated Gene Expression. PLoS ONE, 2011; 6 (7): e22544.

31. Makino Y, Nakamura H, Ikeda E, et al. Hypoxia-inducible factor regulates survival of antigen receptor-driven T cells. J Immunol, 2003; 15: 6534-40.

32. Sanchez AP, Sharma K. Transcription factors in the pathogenesis of diabetic nephropathy. Expert Rev Mol Med, 2009; 11: e13.

33. Iizuka K. Recent progress on the role of ChREBP in glucose and lipid metabolism. Endocr J, 2013; 60 (5): 543-55.

34. Li X, Ponten A, Aase K, et al. PDGF-C is a new protease-activated ligand for the PDGF alpha-receptor. Nat Cell Biol, 2000; 2: 302-9.

35. Ponten A, Li X, Thoren P, et al. Transgenic overexpression of platelet-derived growth factor-C in the mouse heart induces cardiac fibrosis, hypertrophy, and dilated cardiomyopathy. Am J Pathol, 2003; 163: 673-82.

36. Campbell JS, Hughes SD, Gilbertson DG, et al. Platelet-derived growth factor C induces liver fibrosis, steatosis, and hepatocellular carcinoma. Proc Natl Acad Sci USA, 2005; 102: 3389-94.

37. Zhuo Y, Hoyle GW, Shan B, et al. Over-expression of PDGF-C using a lung specific promoter results in abnormal lung development. Transgenic Res, 2006; 15: 543-55.

38. Eitner F, Ostendorf T, Van Roeyen C, et al. Expression of a novel PDGF isoform, PDGF-C, in normal and diseased rat kidney. J Am Soc Nephrol, 2002; 13 (4): 910-7.

39. Eitner F, Ostendorf T, Kretzler M, et al. PDGF-C expression in the developing and normal adult human kidney and in glomerular diseases. J Am Soc Nephrol, 2003; 14 (5):

1145-53.

40. Eitner F, Bücher E, van Roeyen C, et al. PDGF-C is a proinflammatory cytokine that mediates renal interstitial fibrosis. J Am Soc Nephrol, 2008; 19 (2): 281-9.

41. Makino H, Mukoyama M, Sugawara A, et al. Roles of connective tissue growth factor and prostanoids in early streptozotocin-induced diabetic rat kidney: the effect of aspirin treatment. Clin Exp Nephrol, 2003; 7 (1): 33-40.

42. Uehara G, Suzuki D, Toyoda M, et al. Glomerular expression of platelet-derived growth factor (PDGF)-A, -B chain and PDGF receptor-alpha, -beta in human diabetic nephropathy. Clin Exp Nephrol, 2004; 8 (1): 36-42.

43. Nakagawa H, Sasahara M, Haneda M, et al. Immunohistochemical characterization of glomerular PDGF B-chain and PDGF beta-receptor expression in diabetic rats. Diabetes Res Clin Pract, 2000; 48 (2): 87-98.

44. Boor P, van Roeyen CR, Kunter U, et al. PDGF-C mediates glomerular capillary repair. Am J Pathol, 2010; 177 (1): 58-69.

45. Lambers Heerspink HJ, Kwakernaak A, de Zeeuw D, et al. Comment on: Ekinci et al. Dietary salt intake and mortality in patients with type 2 diabetes. Diabetes Care, 2011; 34: 703-709. Diabetes Care, 2011; 34 (7): e124.

46. Caramori ML, Fioretto P, Mauer M. Low glomerular filtration rate in normoalbuminuric type 1 diabetic patients: an indicator of more advanced glomerular lesions. Diabetes, 2003; 52 (4): 1036-40.

47. Kamijo-Ikemori A, Sugaya T, Yasuda T, et al. Clinical significance of urinary liver-type fatty acid-binding protein in diabetic nephropathy of type 2 diabetic patients. Diabetes Care, 2011; 34 (3): 691-6.

48. Ikram MK, Cheung CY, Lorenzi M, et al. Retinal vascular caliber as a biomarker for diabetes microvascular complications. Diabetes Care, 2013; 36 (3): 750-9.

49. Barutta F, Tricarico M, Corbelli A, et al. Urinary Exosomal MicroRNAs in Incipient Diabetic Nephropathy. PLoS One, 2013; 8 (11): e73798.

Legend for Figures

Figure 1

High glucose induces expression of platelet-derived growth factor-C (PDGF-C) via ChREBP in glomerular mesangial cells.

(A, G) Human PDGF-C (*PDGF-C*) (A) or mouse PDGF-C (*Pdgf-c*) (G) gene structure. Exons are shown as boxes and are numbered. (B, H) Human mesangial cells (hMC) (B) or mouse mesangial cells (mMC) (H) were cultured in either normal glucose medium (NG; 5.6 mM) or high glucose medium (HG; 25 mM) for 48 h, and chromatin immunoprecipitation (ChIP) assays using anti-ChREBP antibody were then performed. Rabbit polyclonal IgG (IgG) was applied as a control. PCR products spanning indicated region of PDGF-C gene promoter by 40 cycles were separated by electrophoresis. (C, D) hMC were incubated in NG or HG medium for 48 h. mRNA expression of human *PDGF-C* was determined by real-time PCR. The means ± SD of mRNA levels relative to cells in NG medium are presented. * $P<0.05$; n=4 (C). Immunoblot analyses for expression of human PDGF-C (hPDGF-C) and the mean ± SD of the relative expression level of hPDGF-C to β-actin level. * $P<0.05$; n=4 (D). (E, F) mMC were incubated in the medium containing the indicated concentrations of glucose for 24 h. (E) mRNA expression of mouse *Pdgf-c* was determined by real-time PCR. The means ± SD of mRNA levels relative to cells in NG medium are presented. * $P<0.05$; ** $P<0.01$; n=6. (F) Immunoblot analyses for expression of mouse PDGF-C (mPDGF-C) and the mean ± SD of the relative expression level of mPDGF-C to β-actin level. * $P=0.05$; ** $P<0.05$; n=4. (I) mMC transfected with the small ChREBP hairpin RNA (shRNA) expression vector were incubated for 24 h in either NG or HG medium and the *Pdgf-c* mRNA levels were determined by real-time PCR. An shRNA with non-targeting sequence was used as a control. The means ± SD of the mRNA levels relative to cells in control shRNA-transfected cells in NG medium are presented. * $P<0.05$; ** $P<0.01$; n=4.

Figure 2

PDGF-C is expressed in the glomeruli of diabetic model mouse.

(A) Streptozotocin (STZ)-induced diabetic and control mice were dissected at 0-20 weeks after treatment as indicated, and immunohistochemical analyses for PDGF-C expression in the glomeruli were performed. Bars=20 μm. (B, C) Semiquantitative analyses for PDGF-C positive cells were performed by the counting of 30 glomeruli. (B) The mean ± SD of the number of the positive cells per glomerulus was indicated. * $P<0.05$; ** $P<0.01$; † $P<0.01$ (STZ vs control). (C) The ratio of positive cells to the total number of the counted cells was indicated. * $P<0.05$; ** $P<0.01$; † $P<0.05$ (STZ vs control); $ $P<0.01$ (STZ vs control).

Figure 3

PDGF-C is expressed in mesangial cells in the glomeruli of diabetic model mouse.

(A - C) Immunofluorescent study for PDGF-C, α-smooth muscle actinin (α-SMA) (A), Nephrin (B), and CD34 (C) expression in the glomeruli of streptozotocin (STZ)-induced diabetic mice and control mice at 12 weeks after STZ treatment. Bars=20 μm. 4, 6-diamidino-2-phenylindole (DAPI) signals depict localization of the nucleus. (D) Semi quantitative analyses of the cells co-positive for PDGF-C and for each marker were performed by the counting of 10 glomeruli to determine the ratio of co-positive cells to the total number of the counted cells. * $P<0.1$; ** $P<0.05$; *** $P<0.01$; † $P<0.01$ (STZ vs control).

Figure 4

PDGF-C expression in tubulointerstital area.

Immunohistochemical analyses for PDGF-C expression in kidney of streptozotocin (STZ) induced diabetic mice and control mice were performed. Bars=20 μm.

Figure 5

PDGF-C knockdown reduces high glucose-induced up-regulation of type IV collagen and type VI collagen expression in mesangial cells.

(A - D) Small hairpin RNA (shRNA) targeting PDGF-C was introduced to mouse mesangial cells, and then the cells were incubated in NG or HG medium for 24 h. A non-target shRNA was used as a control. (A) Mouse *Col4a1* (*Col4a1*) mRNA levels were determined by real-time PCR. The means ± SD of the mRNA levels relative to cells in control shRNA-transfected cells in NG medium are presented. * $P<0.05$; ** $P<0.01$; n=5. (B) Mouse *Col6a1* (*Col6a1*) mRNA levels were determined by real-time PCR. The means ± SD of the mRNA levels relative to cells in control shRNA-transfected cells in NG medium are presented. * $P<0.05$; n=5. (C) Mouse type IV collagen (mCol IV) and (D) mouse type VI collagen (mCol VI) expression were determined by immnoblot.

Figure 6

PDGF receptor inhibitor reduces high glucose-induced up-regulation of *Col4a-1* and *Col6a-1* gene expression in mesangial cells.

(A, B) Cultured human mesangial cells were incubated under NG media or under HG media in the presence (+) or absence (-) of 10 μM 6, 7-Dimethyl-2-phenylquinoxaline (AG1295) for 24 h. (A) Real-time PCR analysis of *COL4A1* mRNA expression was performed. The means ± SD of the mRNA levels relative to cells in NG medium are presented. * $P<0.01$; n=7. (B) Real-time PCR analysis of *COL6A1* mRNA expression was performed. The means ± SD of the mRNA levels relative to cells in NG medium are presented. * $P<0.05$; ** $P<0.01$; n=7.

Figure 7

PDGF-C-mediated regulation of type IV collagen or type VI collagen expression in mesangial cells.

(A, B) Cultured human mesangial cells were incubated under NG media in the presence (+) or absence (-) of 40 ng/ml PDGF-C for 24 h. (A) Real-time PCR analysis of *COL4A1* mRNA expression was performed. The mean ± SD of the mRNA levels relative to cells in the absence of PDGF-C was presented. * P<0.01; n=5. (B) Real-time PCR analysis of *COL6A1* mRNA expression was performed. The mean ± SD of the mRNA levels relative to cells in the absence of PDGF-C was presented. * P<0.01; n=5.

Figure 8

Urinary PDGF-C level is increased in diabetic model mice.

(A, B) Urinary albumin (A) or PDGF-C (B) levels of streptozotocin (STZ)-induced diabetic mice and control mice were measured by ELISA at 0-16 weeks after treatment as indicated. Results were expressed as albumin-creatinine ratio (mg/gCr) and PDGF-C-creatinine ratio (ng/gCr). * P<0.01; † P<0.01 (STZ vs control); n=6-14 (A) and * P<0.05; ** P<0.01; † P<0.01 (STZ vs control); n=6-14 (B). (C, D) Urinary albumin (C) or PDGF-C (D) levels of db/db mice and db/m mice were measured at 6-22 weeks after birth. * P<0.1; ** P<0.05; † P<0.01 (db/db vs db/m); n=8-12 (C) and * P<0.1; ** P<0.05; † P<0.05; $ P<0.01; # P<0.1 (db/db vs db/m); n=8-12 (D). (E, F) Plasma PDGF-C levels of STZ induced diabetic mice and control mice (12 weeks after treatment) (E) or db/db mice and db/m mice (14 weeks old) (F) were measured. n=4.

Figure 1

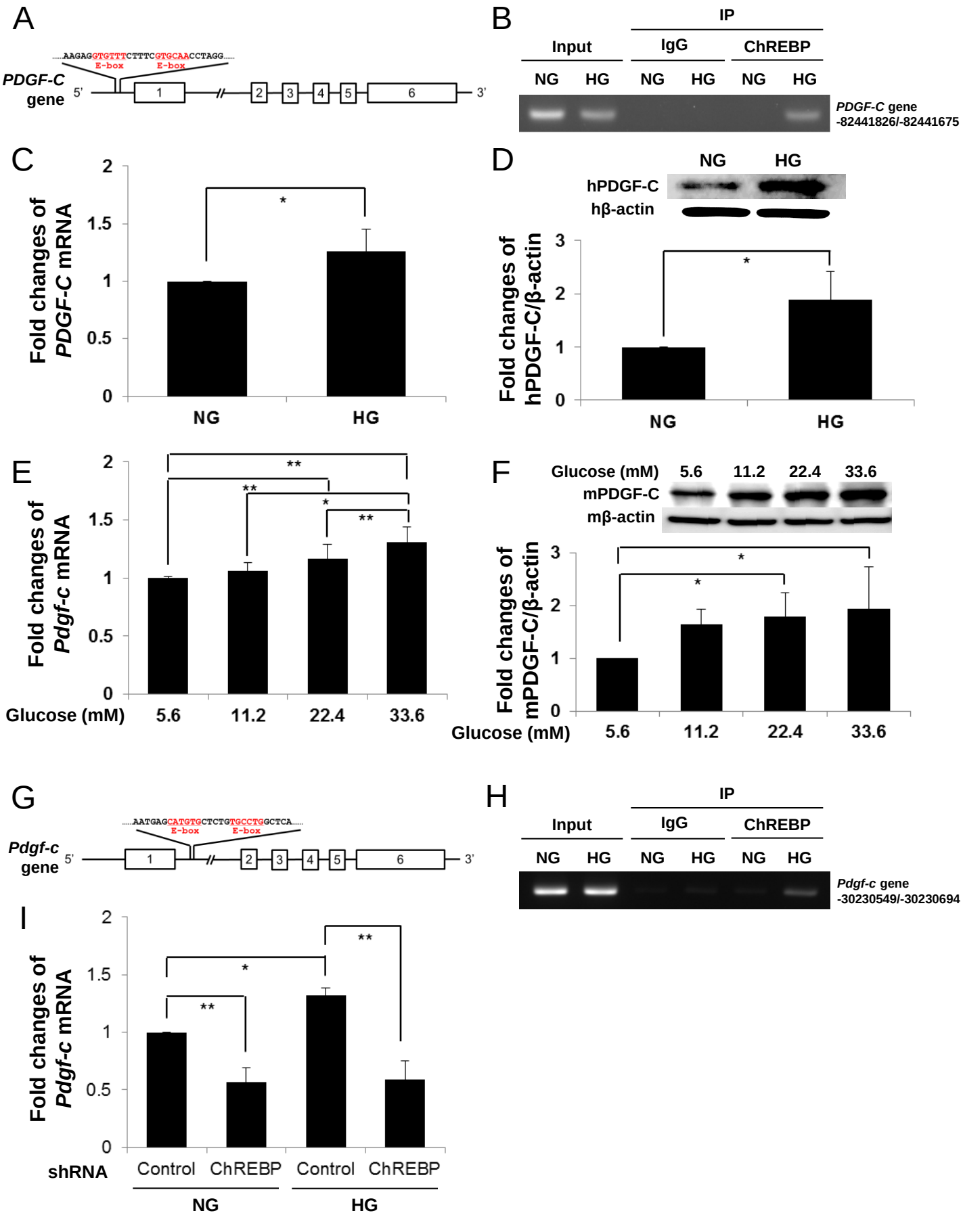
A
AAGAGGTGTTTCTTTCGTGCAACCTAGG
E-box
E-box
PDGF-C gene
5'
1
2
3
4
5
6
3'
B
IP
Input
IgG
ChREBP
NG
HG
NG
HG
NG
HG
PDGF-C gene
-82441826/-82441675
C
Fold changes of PDGF-C mRNA
2
1.5
1
0.5
0
*
NG
HG
D
NG
HG
hPDGF-C
hβ-actin
Fold changes of hPDGF-C/β-actin
3
2
1
0
*
NG
HG
E
Fold changes of Pdgf-c mRNA
2
1.5
1
0.5
0
**
**
*
**
Glucose (mM)
5.6
11.2
22.4
33.6
F
Glucose (mM)
5.6
11.2
22.4
33.6
mPDGF-C
mβ-actin
Fold changes of mPDGF-C/β-actin
3
2
1
0
*
*
Glucose (mM)
5.6
11.2
22.4
33.6
G
AATGAGCATGTGCTCTGTGCCTGGCTCA
E-box
E-box
Pdgf-c gene
5'
1
2
3
4
5
6
3'
H
IP
Input
IgG
ChREBP
NG
HG
NG
HG
NG
HG
Pdgf-c gene
-30230549/-30230694
I
Fold changes of Pdgf-c mRNA
2
1.5
1
0.5
0
*
**
**
shRNA
Control
ChREBP
Control
ChREBP
NG
HG

Figure 2

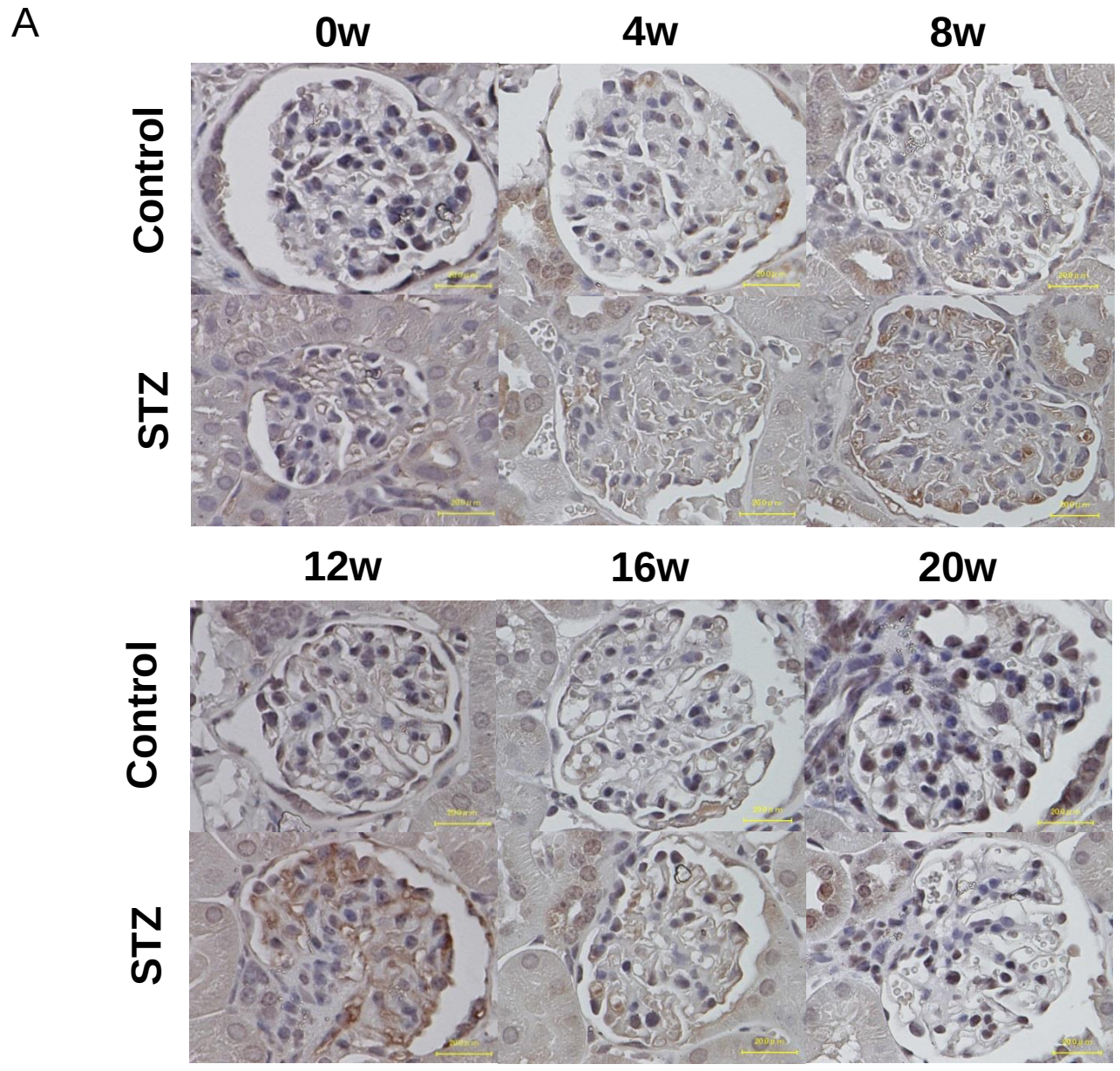
A
0w
4w
8w
Control
STZ
12w
16w
20w
Control
STZ

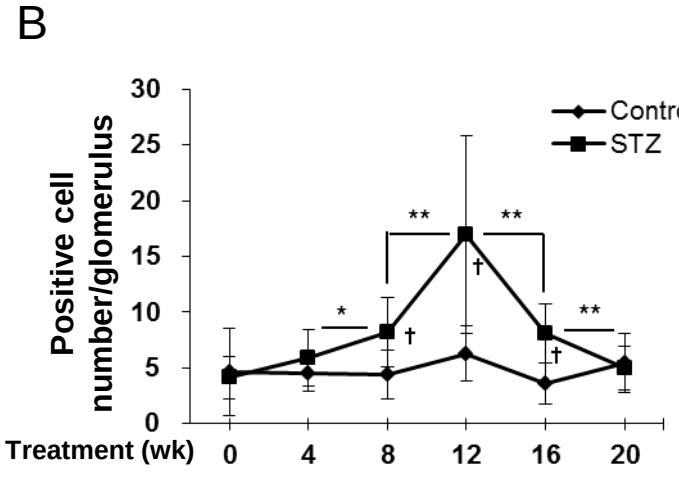
B
Positive cell number/glomerulus
30
25
20
15
10
5
0
Control
STZ
*
**
**
**
†
†
†
Treatment (wk)
0
4
8
12
16
20

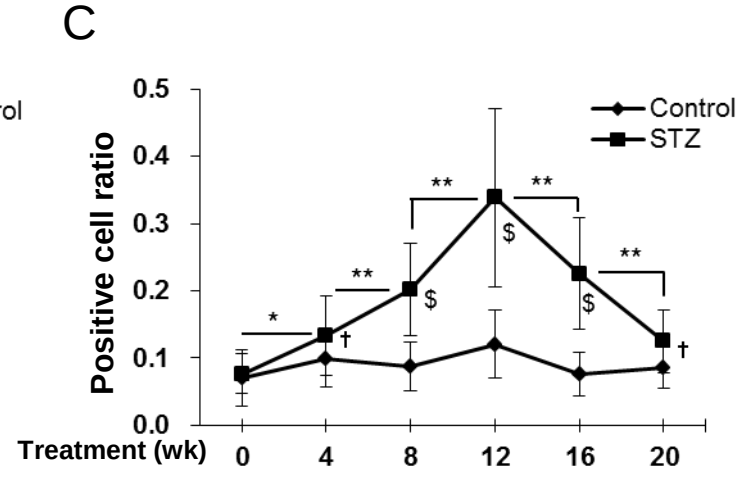
C
Positive cell ratio
0.5
0.4
0.3
0.2
0.1
0.0
Control
STZ
*
**
**
**
**
$
$
$
†
†
Treatment (wk)
0
4
8
12
16
20

Figure 3

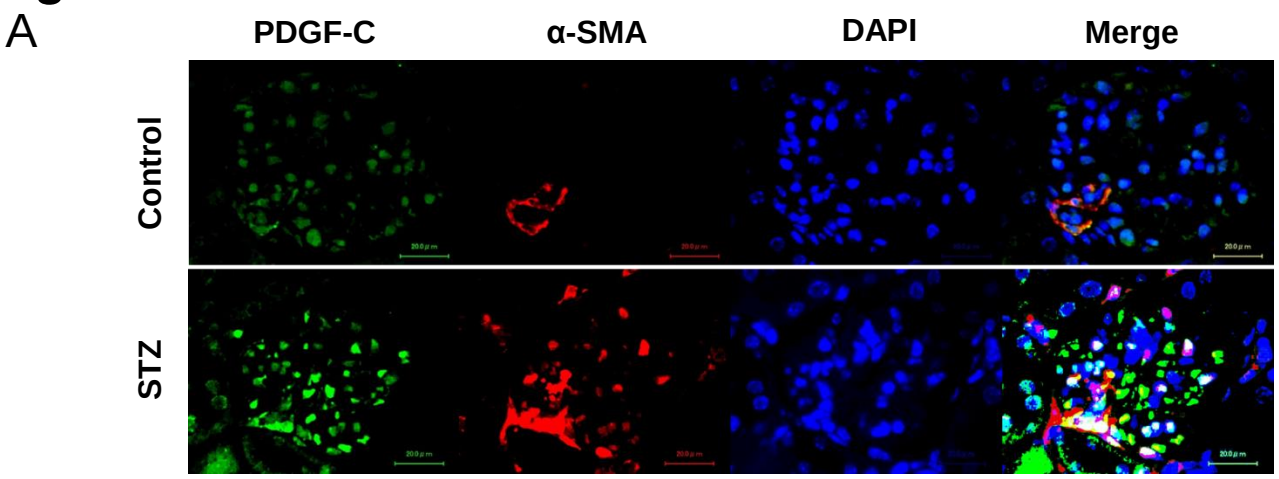
A
PDGF-C
α-SMA
DAPI
Merge
Control
STZ

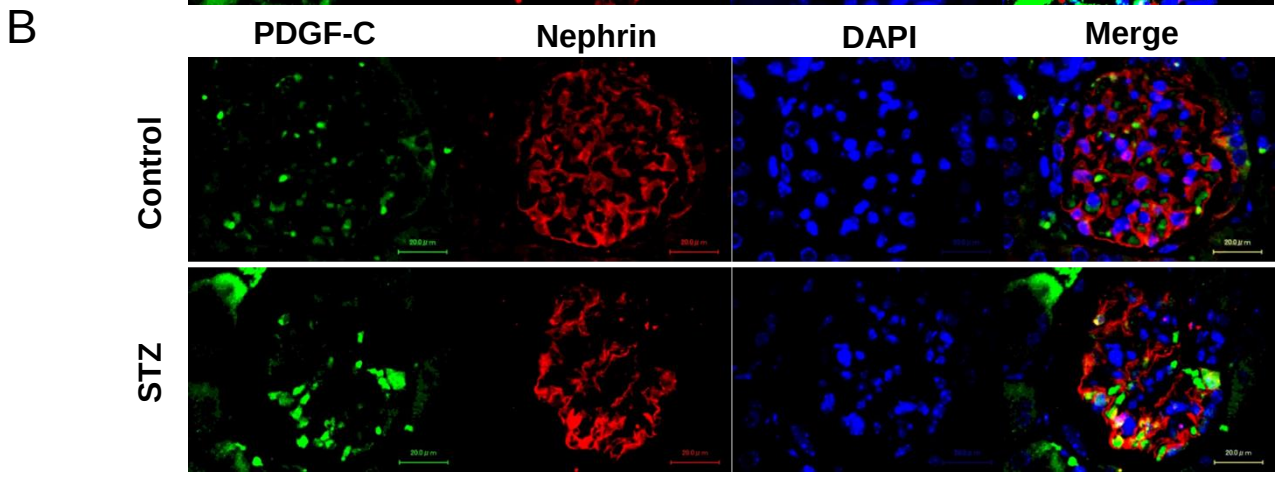
B
PDGF-C
Nephrin
DAPI
Merge
Control
STZ

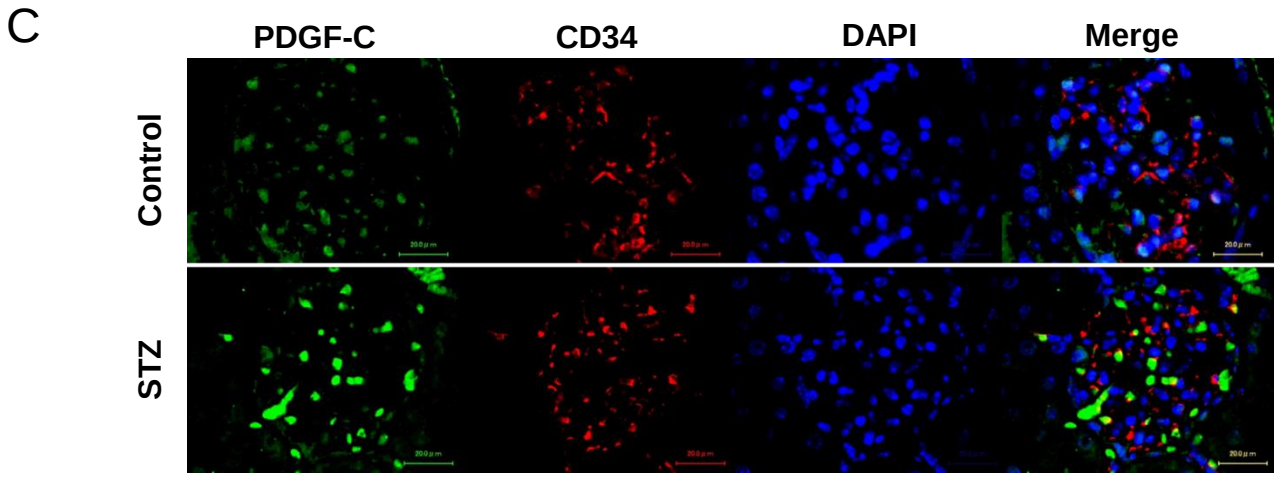
C
PDGF-C
CD34
DAPI
Merge
Control
STZ

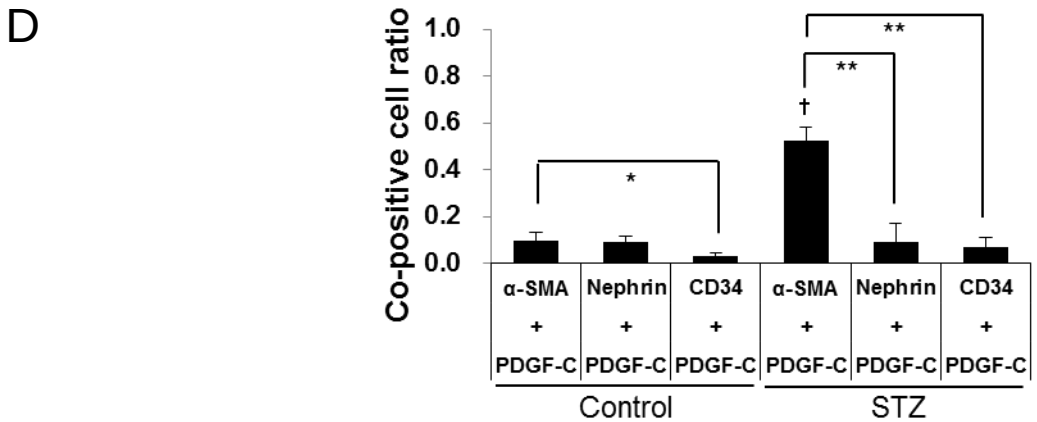
D
Co-positive cell ratio
1.0
0.8
0.6
0.4
0.2
0.0
*
**
**
†
α-SMA + PDGF-C
Nephrin + PDGF-C
CD34 + PDGF-C
α-SMA + PDGF-C
Nephrin + PDGF-C
CD34 + PDGF-C
Control
STZ

Figure 4

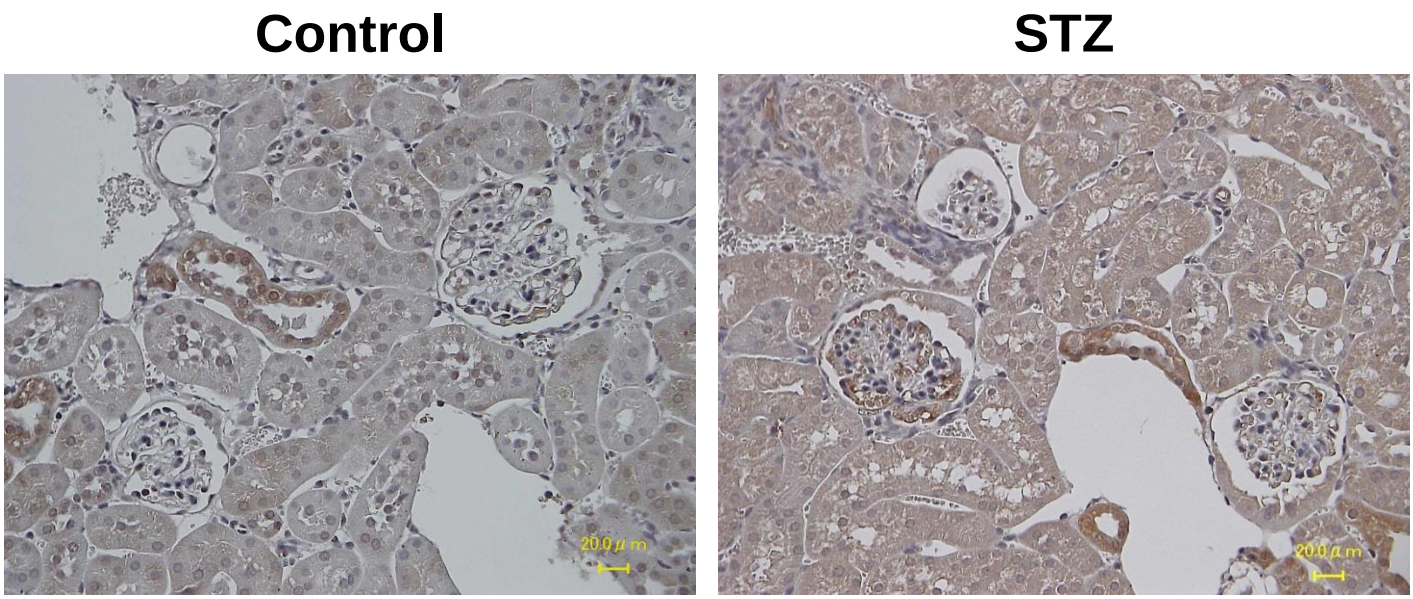

Figure 5

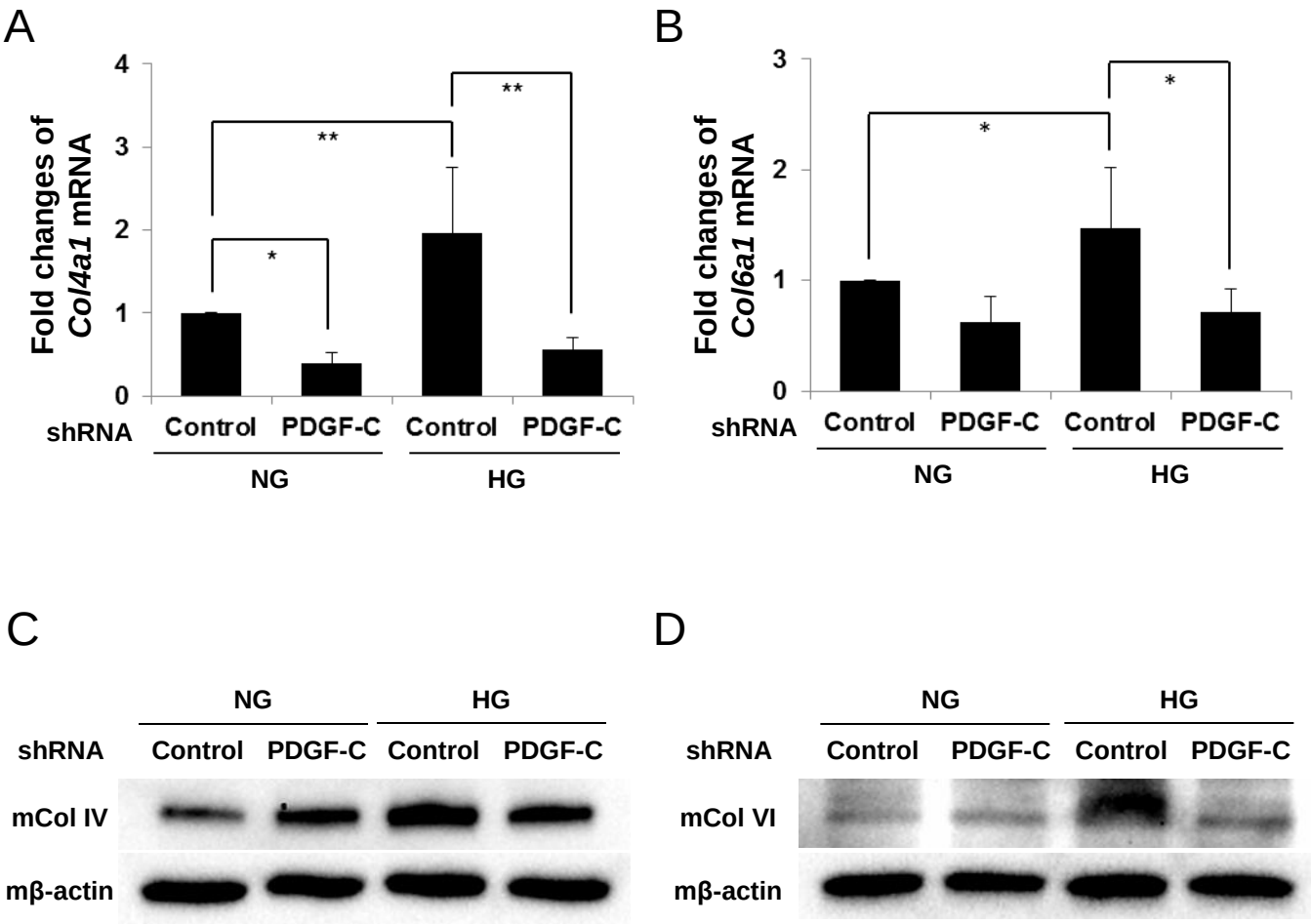
A
Fold changes of Col4a1 mRNA
4
3
2
1
0
**
**
*
shRNA
Control
PDGF-C
Control
PDGF-C
NG
HG
B
Fold changes of Col6a1 mRNA
3
2
1
0
*
*
shRNA
Control
PDGF-C
Control
PDGF-C
NG
HG
C
NG
HG
shRNA
Control
PDGF-C
Control
PDGF-C
mCol IV
mβ-actin
D
NG
HG
shRNA
Control
PDGF-C
Control
PDGF-C
mCol VI
mβ-actin

Figure 6

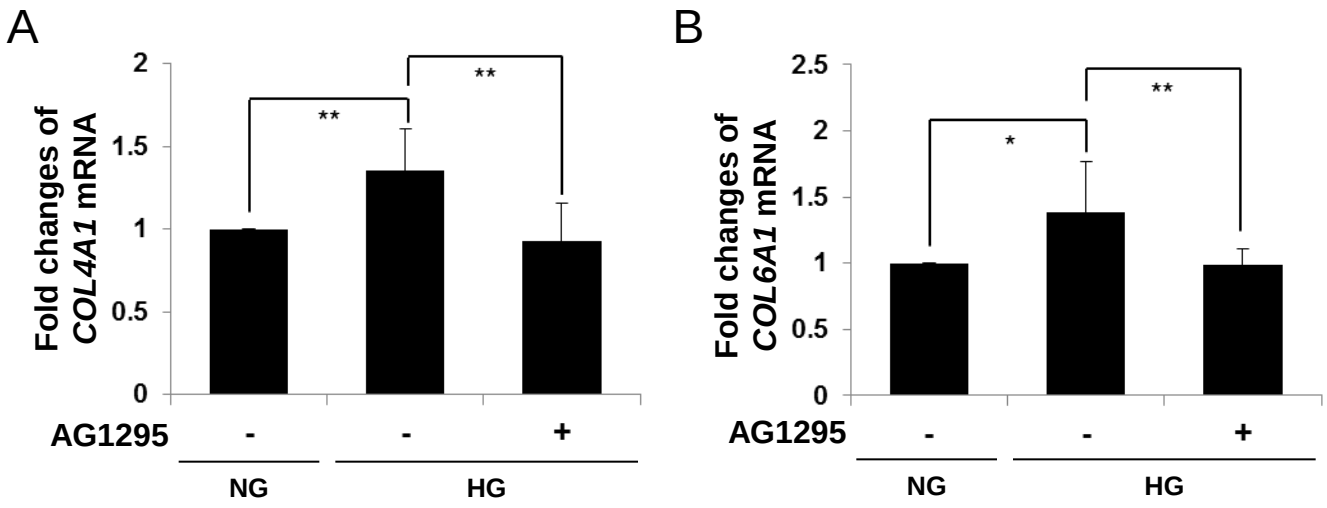
A
Fold changes of COL4A1 mRNA
2
1.5
1
0.5
0
**
**
AG1295
-
-
+
NG
HG
B
Fold changes of COL6A1 mRNA
2.5
2
1.5
1
0.5
0
*
**
AG1295
-
-
+
NG
HG

Figure 7

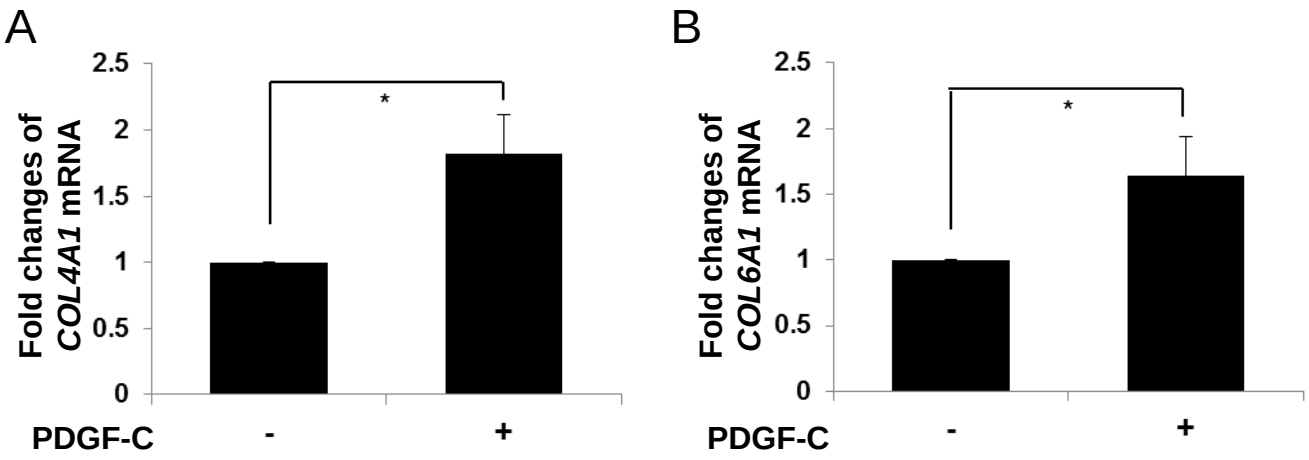
A
Fold changes of COL4A1 mRNA
2.5
2
1.5
1
0.5
0
*
PDGF-C
-
+
B
Fold changes of COL6A1 mRNA
2.5
2
1.5
1
0.5
0
*
PDGF-C
-
+

Figure 8

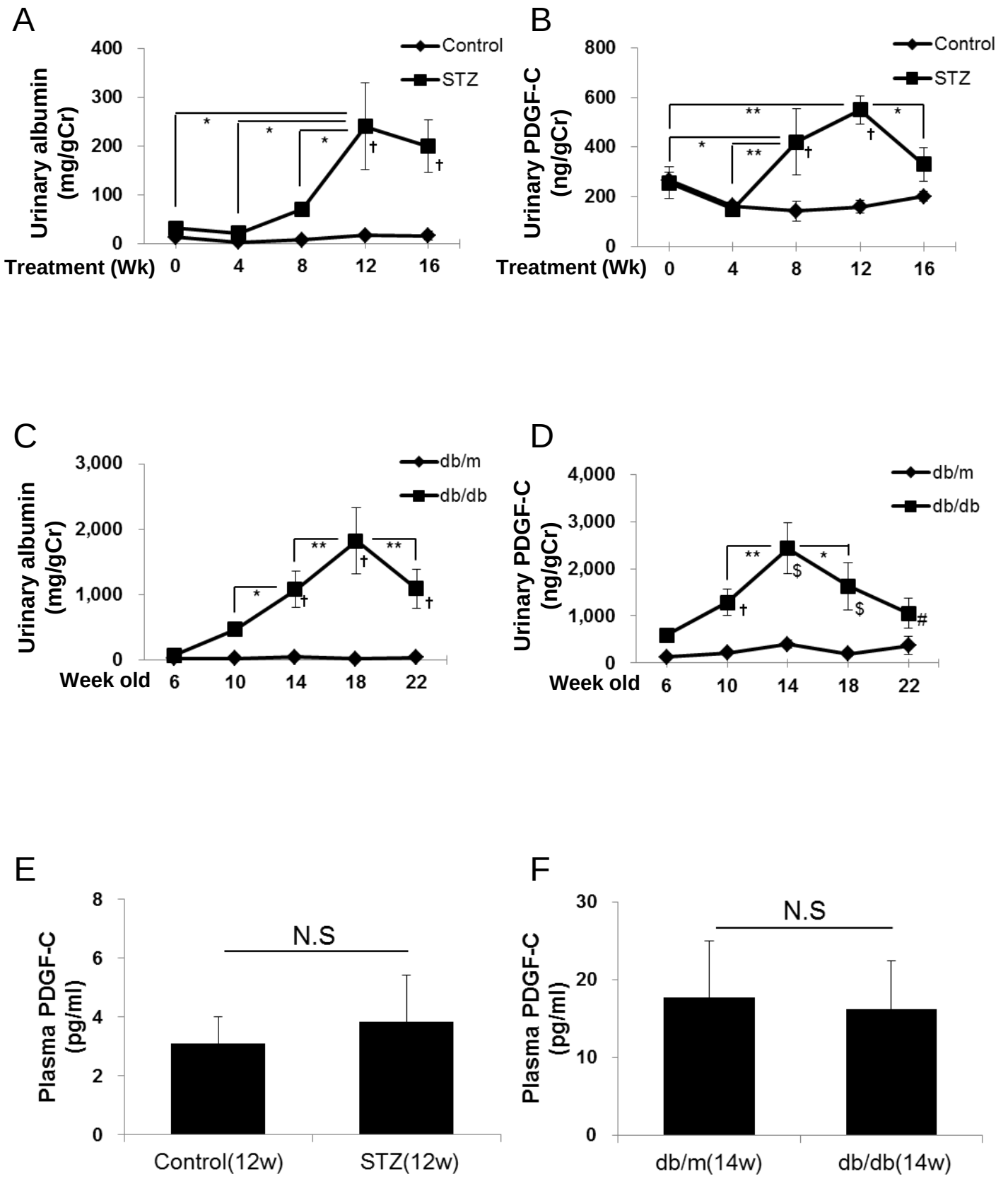
A
Urinary albumin (mg/gCr)
400
300
200
100
0
Control
STZ
Treatment (Wk)
0
4
8
12
16
B
Urinary PDGF-C (ng/gCr)
800
600
400
200
0
Control
STZ
Treatment (Wk)
0
4
8
12
16
C
Urinary albumin (mg/gCr)
3,000
2,000
1,000
0
db/m
db/db
Week old
6
10
14
18
22
D
Urinary PDGF-C (ng/gCr)
4,000
3,000
2,000
1,000
0
db/m
db/db
Week old
6
10
14
18
22
E
Plasma PDGF-C (pg/ml)
8
6
4
2
0
N.S
Control(12w)
STZ(12w)
F
Plasma PDGF-C (pg/ml)
30
20
10
0
N.S
db/m(14w)
db/db(14w)

Table 1 The peak location and the nearest gene list

upstream 5k

chrom	start	end	strand	Interval Analysis	nearGeneID	nearGene Symbol	Description
chr9	139887061	139892061	+	chr9:139888821-139889217	NM_000718	CACNA1B	calcium channel, voltage-dependent, N type, alpha 1B subunit
chr10	80937362	80942362	+	chr10:80936795-80937387	NM_001099692	EIF5AL1	eukaryotic translation initiation factor 5A-like 1
chr20	52120711	52125711	-	chr20:52122809-52123187	NM_003657	BCAS1	breast carcinoma amplified sequence 1
chr22	48946286	48951286	+	chr22:48946543-48946925	NM_052839	PANX2	pannexin 2
chr22	48946286	48951286	+	chr22:48946543-48946925	NM_001160300	PANX2	pannexin 2
chr22	48946286	48951286	+	chr22:48946543-48946925	NR_027691	PANX2	pannexin 2

downstream 5k

chr.	start	end	strand	Interval Analysis	nearGeneID	nearGene Symbol	Description
chr1	67031011	67036011	-	chr1:67034492-67034733	NM_005478	INSL5	insulin-like 5
chr4	157897213	157902213	-	chr4:157900155-157900677	NM_016205	PDGFC	platelet derived growth factor C
chr6	20203913	20208913	-	chr6:20206023-20206246	NM_001080480	MBOAT1	membrane bound O-acyltransferase domain containing 1
chr10	76606455	76611455	+	chr10:76606875-76607087	NM_144660	SAMD8	sterile alpha motif domain containing 8
chr16	82639869	82644869	-	chr16:82642023-82643078	NM_003791	MBTPS1	membrane-bound transcription factor peptidase, site 1
chr22	34459728	34464728	-	chr22:34460947-34461159	NM_001082576	RBFOX2	RNA binding protein, fox-1 homolog (C. elegans) 2
chr22	34459728	34464728	-	chr22:34460947-34461159	NM_001082579	RBFOX2	RNA binding protein, fox-1 homolog (C. elegans) 2
chr22	34459728	34464728	-	chr22:34460947-34461159	NM_001082578	RBFOX2	RNA binding protein, fox-1 homolog (C. elegans) 2
chr22	34459728	34464728	-	chr22:34460947-34461159	NM_014309	RBFOX2	RNA binding protein, fox-1 homolog (C. elegans) 2
chr22	34459728	34464728	-	chr22:34460947-34461159	NM_001082577	RBFOX2	RNA binding protein, fox-1 homolog (C. elegans) 2
chr22	34459728	34464728	-	chr22:34460947-34461159	NM_001031695	RBFOX2	RNA binding protein, fox-1 homolog (C. elegans) 2
chr22	48942242	48947242	+	chr22:48946543-48946925	NM_018995	MOV10L1	Mov10l1, Moloney leukemia virus 10-like 1, homolog (mouse)
chr22	48942242	48947242	+	chr22:48946543-48946925	NM_001164104	MOV10L1	Mov10l1, Moloney leukemia virus 10-like 1, homolog (mouse)
chr22	48942242	48947242	+	chr22:48946543-48946925	NM_001164105	MOV10L1	Mov10l1, Moloney leukemia virus 10-like 1, homolog (mouse)
chr22	48942242	48947242	+	chr22:48946543-48946925	NM_001164106	MOV10L1	Mov10l1, Moloney leukemia virus 10-like 1, homolog (mouse)
chr22	49530593	49535593	+	chr22:49533706-49534095	NM_001097	ACR	acrosin

gene(include intron)

chr.	start	end	strand	Interval Analysis	nearGeneID	nearGene Symbol	Description
chr1	6767970	7752351	+	chr1:7050114-7050318	NM_015215	CAMTA1	calmodulin binding transcription activator 1
chr1	107915304	108309068	-	chr1:107962398-107962639	NM_006113	VAV3	vav 3 guanine nucleotide exchange factor
chr1	107915304	108032649	-	chr1:107962398-107962639	NM_001079874	VAV3	vav 3 guanine nucleotide exchange factor
chr1	175104576	175400647	-	chr1:175278964-175279366	NM_207108	ASTN1	astrotactin 1
chr1	175096825	175400647	-	chr1:175278964-175279366	NM_004319	ASTN1	astrotactin 1
chr1	2149993	2231511	+	chr1:2202788-2203608	NM_003036	SKI	v-ski sarcoma viral oncogene homolog
chr1	39319704	39725376	+	chr1:39438001-39438319	NM_012090	MACF1	microtubule-actin crosslinking factor 1
chr1	45254662	45444837	-	chr1:45357961-45358176	NM_020883	ZSWIM5	zinc finger, SWIM-type containing 5
chr1	71090623	71286079	-	chr1:71175517-71175780	NR_028294	PTGER3	prostaglandin E receptor 3 (subtype EP3)
chr1	71090623	71286079	-	chr1:71175517-71175780	NM_198714	PTGER3	prostaglandin E receptor 3 (subtype EP3)
chr1	71090623	71286079	-	chr1:71175517-71175780	NM_198716	PTGER3	prostaglandin E receptor 3 (subtype EP3)
chr1	71090623	71286079	-	chr1:71175517-71175780	NM_198717	PTGER3	prostaglandin E receptor 3 (subtype EP3)
chr1	71090623	71286079	-	chr1:71175517-71175780	NR_028292	PTGER3	prostaglandin E receptor 3 (subtype EP3)
chr1	71090623	71286079	-	chr1:71175517-71175780	NR_028293	PTGER3	prostaglandin E receptor 3 (subtype EP3)
chr1	103114610	103346640	-	chr1:103268286-103268625	NM_080630	COL11A1	collagen, type XI, alpha 1
chr1	103114610	103346640	-	chr1:103268286-103268625	NM_001854	COL11A1	collagen, type XI, alpha 1
chr1	103114610	103346640	-	chr1:103268286-103268625	NM_080629	COL11A1	collagen, type XI, alpha 1
chr1	199884072	200062725	+	chr1:199925994-199926287	NM_020443	NAV1	neuron navigator 1
chr1	242691295	242870283	+	chr1:242716532-242717145	NM_173807	C1orf101	chromosome 1 open reading frame 101
chr1	242691295	242870283	+	chr1:242716532-242717145	NM_001130957	C1orf101	chromosome 1 open reading frame 101
chr1	1099148	1123176	+	chr1:1117691-1118017	NM_001130045	TTLL10	tubulin tyrosine ligase-like family, member 10
chr1	25098588	25164088	-	chr1:25106897-25107273	NM_001031680	RUNX3	runt-related transcription factor 3
chr1	25098588	25129357	-	chr1:25106897-25107273	NM_004350	RUNX3	runt-related transcription factor 3
chr1	26310854	26324611	+	chr1:26317865-26318175	NM_152835	PDIK1L	PDLIM1 interacting kinase 1 like
chr1	26310242	26324611	+	chr1:26317865-26318175	NR_026685	PDIK1L	PDLIM1 interacting kinase 1 like
chr1	26310854	26324611	+	chr1:26317865-26318175	NR_026686	PDIK1L	PDLIM1 interacting kinase 1 like
chr1	86785346	86819020	+	chr1:86799543-86800117	NM_012128	CLCA4	chloride channel accessory 4
chr1	86785346	86819018	+	chr1:86799543-86800117	NR_024602	CLCA4	chloride channel accessory 4
chr2	936553	1350389	+	chr2:995023-995238	NM_018968	SNTG2	syntrophin, gamma 2
chr2	1397186	1525505	+	chr2:1400327-1400648	NM_175721	TPO	thyroid peroxidase
chr2	1397186	1525505	+	chr2:1400327-1400648	NM_175722	TPO	thyroid peroxidase
chr2	1396239	1525505	+	chr2:1400327-1400648	NM_175719	TPO	thyroid peroxidase
chr2	1396239	1525505	+	chr2:1400327-1400648	NM_000547	TPO	thyroid peroxidase
chr2	1614665	1727298	-	chr2:1678242-1678631	NM_012293	PXDN	peroxidasin homolog (Drosophila)
chr2	29269143	29997936	-	chr2:29500550-29500831	NM_004304	ALK	anaplastic lymphoma receptor tyrosine kinase
chr2	152050100	152299247	-	chr2:152289616-152289833	NM_004543	NEB	nebulin
chr2	152050100	152299247	-	chr2:152289616-152289833	NM_001164508	NEB	nebulin
chr2	152050100	152299247	-	chr2:152289616-152289833	NM_001164507	NEB	nebulin
chr2	162189090	162550032	+	chr2:162473446-162473755	NM_022058	SLC4A10	solute carrier family 4, sodium bicarbonate transporter, member 10
chr3	54131732	55083624	+	chr3:54976692-54976975	NM_018398	CACNA2D3	calcium channel, voltage-dependent, alpha 2/delta subunit 3
chr3	85090822	86206267	+	chr3:85593565-85593790	NM_001167674	CADM2	cell adhesion molecule 2
chr3	85090822	86206267	+	chr3:85593565-85593790	NM_001167675	CADM2	cell adhesion molecule 2
chr3	174598937	175483810	+	chr3:174823243-174823633	NM_014932	NLGN1	neuroligin 1
chr3	185120417	185218421	-	chr3:185157145-185157570	NM_005688	ABCC5	ATP-binding cassette, sub-family C (CFTR/MRP), member 5
chr3	193342377	193928082	-	chr3:193535519-193535761	NM_004113	FGF12	fibroblast growth factor 12
chr3	193342377	193609532	-	chr3:193535519-193535761	NM_021032	FGF12	fibroblast growth factor 12
chr3	46370238	46375872	+	chr3:46371377-46371702	NM_001123396	CCR2	chemokine (C-C motif) receptor 2
chr3	46370238	46377417	+	chr3:46371377-46371702	NM_001123041	CCR2	chemokine (C-C motif) receptor 2
chr4	23402741	23500798	-	chr4:23487607-23487917	NM_013261	PPARGC1A	peroxisome proliferator-activated receptor gamma, coactivator 1 alpha
chr4	140806371	140844856	+	chr4:140844341-140844562	NM_002413	MGST2	microsomal glutathione S-transferase 2
chr4	187691802	187713531	-	chr4:187705074-187705325	NM_005958	MTNR1A	melatonin receptor 1A
chr5	357290	491405	+	chr5:450286-451258	NM_020731	AHRR	aryl-hydrocarbon receptor repressor
chr6	5206582	5716815	+	chr6:5527184-5527516	NM_006567	FARS2	phenylalanyl-tRNA synthetase 2, mitochondrial
chr6	161688579	163068824	-	chr6:162937576-162937795	NM_013988	PARK2	parkinson protein 2, E3 ubiquitin protein ligase (parkin)

chr6	161688579	163068824	-	chr6:162937576-162937795	NM_004562	PARK2	parkinson protein 2, E3 ubiquitin protein ligase (parkin)
chr6	161688579	163068824	-	chr6:162937576-162937795	NM_013987	PARK2	parkinson protein 2, E3 ubiquitin protein ligase (parkin)
chr6	430137	638109	-	chr6:621342-621786	NM_018303	EXOC2	exocyst complex component 2
chr6	166742843	167195761	-	chr6:167117439-167117687	NM_001006932	RPS6KA2	ribosomal protein S6 kinase, 90kDa, polypeptide 2
chr7	157024510	158073243	-	chr7:157181550-157181858	NM_130842	PTPRN2	protein tyrosine phosphatase, receptor type, N polypeptide 2
chr7	157024510	158073243	-	chr7:157181550-157181858	NM_002847	PTPRN2	protein tyrosine phosphatase, receptor type, N polypeptide 2
chr7	157024510	158073243	-	chr7:157181550-157181858	NM_130843	PTPRN2	protein tyrosine phosphatase, receptor type, N polypeptide 2
chr7	904062	960815	-	chr7:940004-940213	NM_006869	ADAP1	ArfGAP with dual PH domains 1
chr8	1436975	1644049	+	chr8:1578676-1579082	NM_004745	DLGAP2	discs, large (Drosophila) homolog-associated protein 2
chr8	1980564	2080787	+	chr8:2021208-2021485	NM_003970	MYOM2	myomesin 2
chr8	108330885	108579430	-	chr8:108342167-108342418	NM_001146	ANGPT1	angiopoietin 1
chr9	93524704	93752265	-	chr9:93598954-93599373	NM_004560	ROR2	receptor tyrosine kinase-like orphan receptor 2
chr9	5774571	5823081	-	chr9:5795862-5796185	NM_024896	ERMP1	endoplasmic reticulum metallopeptidase 1
chr9	126680394	126743207	-	chr9:126697764-126698066	NM_002077	GOLGA1	golgin A1
chr9	139101237	139123460	+	chr9:139116270-139116543	NM_016219	MAN1B1	mannosidase, alpha, class 1B, member 1
chrX	8392870	8394551	+	chrX:8394088-8394330	NM_001001888	VCX3B	variable charge, X-linked 3B
chrX	31047265	33267647	-	chrX:33147422-33147669	NM_000109	DMD	dystrophin
chrX	36163971	36313354	+	chrX:36261417-36261636	NM_001098843	CXorf30	chromosome X open reading frame 30
chrX	51562894	51662190	+	chrX:51616965-51617210	NM_001005332	MAGED1	melanoma antigen family D, 1
chrX	53575796	53730398	-	chrX:53577848-53578066	NM_031407	HUWE1	HECT, UBA and WWE domain containing 1
chrX	139693090	139694389	-	chrX:139693164-139694042	NM_004065	CDR1	cerebellar degeneration-related protein 1, 34kDa
chr10	310131	725608	-	chr10:549877-550227	NM_014974	DIP2C	DIP2 disco-interacting protein 2 homolog C (Drosophila)
chr11	68572925	68614648	+	chr11:68592613-68592843	NM_139075	TPCN2	two pore segment channel 2
chr11	73560015	73643396	+	chr11:73624902-73625216	NM_016147	PPME1	protein phosphatase methylesterase 1
chr12	77782579	78369918	+	chr12:78297526-78297773	NM_005639	SYT1	synaptotagmin I
chr12	77781903	78369918	+	chr12:78297526-78297773	NM_001135805	SYT1	synaptotagmin I
chr12	77963563	78369918	+	chr12:78297526-78297773	NM_001135806	SYT1	synaptotagmin I
chr12	128122223	128954165	-	chr12:128139104-128139448	NM_133448	TMEM132D	transmembrane protein 132D
chr13	112392643	112589483	+	chr13:112565521-112565825	NM_032189	ATP11A	ATPase, class VI, type 11A
chr13	112392643	112589483	+	chr13:112565521-112565825	NM_015205	ATP11A	ATPase, class VI, type 11A
chr14	89333221	89490842	-	chr14:89480604-89480896	NM_145231	EFCAB11	EF-hand calcium binding domain 11
chr15	27001131	27197808	+	chr15:27142644-27142982	NM_005503	APBA2	amyloid beta (A4) precursor protein-binding, family A, member 2
chr15	27001131	27197808	+	chr15:27142644-27142982	NM_001130414	APBA2	amyloid beta (A4) precursor protein-binding, family A, member 2
chr15	98758122	98902448	-	chr15:98797274-98797634	NM_178842	CERS3	ceramide synthase 3
chr16	87861535	88084470	-	chr16:88023460-88024282	NM_013275	ANKRD11	ankyrin repeat domain 11
chr16	2145799	2168131	+	chr16:2154322-2154609	NM_032271	TRAF7	TNF receptor-associated factor 7
chr18	13208785	13642753	+	chr18:13252239-13252457	NM_181482	LDLRAD4	low density lipoprotein receptor class A domain containing 4
chr18	13208785	13642753	+	chr18:13252239-13252457	NM_181481	LDLRAD4	low density lipoprotein receptor class A domain containing 4
chr18	22699269	22769908	+	chr18:22708969-22709363	NR_026908	AQP4-AS1	AQP4 antisense RNA 1
chr18	72665103	72811670	+	chr18:72780853-72781148	NM_007345	ZNF236	zinc finger protein 236
chr18	74930384	75239270	+	chr18:75106703-75106953	NM_198531	ATP9B	ATPase, class II, type 9B
chr18	75256759	75390311	+	chr18:75342986-75344860	NM_006162	NFATC1	nuclear factor of activated T-cells, cytoplasmic, calcineurin-dependent 1
chr18	75256759	75390311	+	chr18:75342986-75344860	NM_172388	NFATC1	nuclear factor of activated T-cells, cytoplasmic, calcineurin-dependent 1
chr18	75261313	75390311	+	chr18:75342986-75344860	NM_172389	NFATC1	nuclear factor of activated T-cells, cytoplasmic, calcineurin-dependent 1
chr18	75261313	75390311	+	chr18:75342986-75344860	NM_172387	NFATC1	nuclear factor of activated T-cells, cytoplasmic, calcineurin-dependent 1
chr19	256574	295791	-	chr19:263529-263843	NM_017550	MIER2	mesoderm induction early response 1, family member 2
chr19	43616179	43770044	+	chr19:43722985-43723233	NM_001042723	RYR1	ryanodine receptor 1 (skeletal)
chr19	43616179	43770044	+	chr19:43722985-43723233	NM_000540	RYR1	ryanodine receptor 1 (skeletal)
chr19	61039755	61085032	+	chr19:61053494-61053695	NM_134444	NLRP4	NLR family, pyrin domain containing 4
chr19	60294092	60320739	-	chr19:60300145-60300676	NM_017607	PPP1R12C	protein phosphatase 1, regulatory subunit 12C
chr19	61344367	61364074	+	chr19:61353978-61354610	NM_018337	ZNF444	zinc finger protein 444
chr21	46094302	46186796	+	chr21:46168728-46168966	NM_020528	PCBP3	poly(rC) binding protein 3
chr21	46094302	46186796	+	chr21:46168728-46168966	NM_001130141	PCBP3	poly(rC) binding protein 3
chr21	21292503	21833085	+	chr21:21491715-21491932	NM_004540	NCAM2	neural cell adhesion molecule 2
chr21	27212102	27261310	-	chr21:27221225-27221439	NM_007038	ADAMTS5	ADAM metallopeptidase with thrombospondin type 1 motif, 5
chr22	16596905	16637258	-	chr22:16616712-16616945	NM_197967	BID	BH3 interacting domain death agonist
chr22	16596905	16636779	-	chr22:16616712-16616945	NM_197966	BID	BH3 interacting domain death agonist
chr22	16596905	16637258	-	chr22:16616712-16616945	NM_001196	BID	BH3 interacting domain death agonist
chr22	33983444	34021799	+	chr22:33987999-33988247	NM_001003681	HMGXB4	HMG box domain containing 4
chr22	33983444	34021799	+	chr22:33987999-33988247	NR_027780	HMGXB4	HMG box domain containing 4
chr22	48839946	48865908	-	chr22:48847906-48848226	NM_139202	MLC1	megalencephalic leukoencephalopathy with subcortical cysts 1
chr22	48839946	48866485	-	chr22:48847906-48848226	NM_015166	MLC1	megalencephalic leukoencephalopathy with subcortical cysts 1
chr22	48998244	49025527	-	chr22:49014839-49015363	NM_020461	TUBGCP6	tubulin, gamma complex associated protein 6